


# Geometrical Effect on Thermal Conductivity of Unidirectional Fiber-Reinforced Polymer Composite along Different In-plane Orientations

Zenong Fang<sup>1</sup> · Min Li<sup>1</sup> · Shaokai Wang<sup>1</sup>  · Yanxia Li<sup>1</sup> · Xiaolei Wang<sup>2</sup> · Yizhuo Gu<sup>1</sup> · Qianli Liu<sup>2</sup> · Jie Tian<sup>2</sup> · Zuoguang Zhang<sup>1</sup>

Received: 18 October 2017 / Accepted: 25 October 2017 / Published online: 14 November 2017  
© Springer Science+Business Media B.V. 2017

**Abstract** This paper focuses on the anisotropic characteristics of the in-plane thermal conductivity of fiber-reinforced polymer composite based on experiment and simulation. Thermal conductivity along different in-plane orientations was measured by laser flash analysis (LFA) and steady-state heat flow method. Their heat transfer processes were simulated to reveal the geometrical effect on thermal conduction. The results show that the in-plane thermal conduction of unidirectional carbon-fiber-reinforced polymer composite is greatly influenced by the sample geometry at an in-plane orientation angle between  $0^\circ$  to  $90^\circ$ . By defining radius-to-thickness as a dimensionless shape factor for the LFA sample, the apparent thermal conductivity shows a dramatic change when the shape factor is close to the tangent of the orientation angle ( $\tan\theta$ ). Based on finite element analysis, this phenomenon was revealed to correlate with the change of the heat transfer process. When the shape factor is larger than  $\tan\theta$ , the apparent thermal conductivity is consistent with the estimated value according to the theoretical model. For a sample with a shape factor smaller than  $\tan\theta$ , the apparent thermal conductivity shows a slow growth around a low value, which seriously deviates from the theory estimation. This phenomenon was revealed to correlate with the change of the heat transfer process from a continuous path to a zigzag path. These results will be helpful in optimizing the ply scheme of composite laminates for thermal management applications.

---

✉ Shaokai Wang  
wsk@buaa.edu.cn

<sup>1</sup> Key Laboratory of Aerospace Advanced Materials and Performance (Ministry of Education), School of Materials Science and Engineering, Beihang University, No. 37 Xueyuan Road, Haidian District, Beijing 100191, China

<sup>2</sup> Shanghai Composite Science & Technology Co., Ltd., No. 3636, Zhaolou Road, Minhang District, Shanghai 201112, China

**Keywords** Carbon-fiber-reinforced polymer composite · Thermal conductivity · Laser flash analysis · Finite element simulation

## 1 Introduction

Polymer composites possess numerous advantages such as lightweight, superior mechanical performance, designability, and multifunctionality [1–8]. In particular, carbon-fiber-reinforced polymer composite (CFRP) has become a primary structural material in applications of aeronautics and astronautics [9–11]. With the development of internal electronic systems toward high integration, heat dissipation and radiation have become major problems for traditional polymer composites [12–14]. Although some high-performance reinforcements, e. g., carbon nanotubes and pitch-based carbon fibers, exhibit excellent thermal conductivity, the anisotropic features of these reinforcements still easily cause poor thermal conductivity in final composite components [15–17]. In order to fully achieve the potential performance of these highly thermal conductive reinforcements, reasonable design and accurate characterization are very important [18, 19]. It is well known that the anisotropy of fiber reinforcement greatly influences the thermal conductivity of polymer composite. The anisotropic microstructure generates many challenges with regard to the characterization and simulation of thermal conductivity [20]. Owing to the complexity of CFRP's microstructure, its in-plane thermal conductivity along a certain direction was normally measured by the steady-state heat flow method or by making a sample suitable for the through-thickness test mode in laser flash analysis (LFA). A group of bars were machined from composite material, stacked, and held together to prepare a square sample, thus ensuring the direction of interest along the sample's thickness direction [21]. Thermal diffusivity can be directly measured by the LFA method [22]. Thermal conductivity can be further calculated from the parameters of thermal diffusivity, specific heat, and the density of the sample. Jiao *et al.* investigated the effects of weave density and fabric architecture of 3D woven composite on thermal conductivity by multi-scale finite element simulation [19]. Robitaille *et al.* designed proper simulative models for CFRP made from three types of reinforcements (tape prepreg, unidirectional fabric, and woven prepreg) to predict the in-plane and through-thickness thermal conductivity based on principles of the steady-state heat flow method. These results indicated the significant influence of different geometric characteristics of reinforcements on the composite's thermal conductivity [23]. Webb *et al.* attempted to measure and calculate the thermal conductivity of CFRP at different fiber angles by a steady-state heat flow method. The deviation between the experimental results and the Springer-Tsai theory was well modified at a fiber orientation angle below 30° [21].

Meanwhile, the simulation of the heat transfer in CFRP during LFA measurement generated more and more attention. McMasters discussed the applicability of LFA measurement on the axial thermal conductivity of carbon-bonded carbon fiber [24]. It was found that recording the temperature at the sample center led to a more reliable thermal diffusivity than mapping the temperature of the entire surface during LFA measurement. Alway-Cooper simulated the axial thermal conductivity of unidirectional CFRP according to principle of LFA. They found that even for the axial thermal conductivity of unidirectional CFRP, the deviation of heat transfer from a one-dimensional assumption may cause an inaccurate estimation of the fiber's thermal conductivity [25]. Based on the principle of LFA, Li *et al.* established finite element method (FEM) to analyze heat conduction in composites and to predict the axial thermal conductivity

of carbon fiber and the interfacial thermal resistance between the fibers and the matrix [26]. This method is also enlightening for simulations on the thermal conductivity of CFRP. In addition to the axial thermal conductivity, the thermal conductivities in other orientations play important roles in heat dissipation [27]. It is necessary to accurately measure and predict the heat transfer along different orientations.

This paper used two methods to measure the in-plane thermal conductivity along different in-plane orientations based on LFA and the steady-state heat flow method. By comparing the experimental results with theoretical calculations, the geometrical effect for the measurement of anisotropic CFRP was found. FEM was further developed to simulate the heat transfer and to analyze the major control factors of the geometrical effect. The investigation of the geometrical effect was helpful in achieving an accurate thermal conductivity characterization of CFRP and in optimizing a ply scheme for composite laminate.

## 2 Experiment

### 2.1 Materials

Pitch-based carbon fiber XN-90-60S, a domestic high-modulus carbon fiber, and epoxy resin AG80 were used to prepare unidirectional CFRP. XN-90-60S were manufactured by Nippon Graphite Fiber Corporation. AG80resin was purchased from the Shanghai Research Institute of Synthetic Resins. Acetone was purchased from Beijing Chemical Works and was used to dissolve AG80. The material properties are listed in Table 1.

### 2.2 Preparation of Unidirectional CFRP Laminate

Carbon fiber prepreg was prepared by a solution method, and the resin content was controlled at 40%. To meet the sample requirement for LFA measurement, 100 layers of prepreg were laid unidirectionally to prepare a thick panel, and then were hot pressed following a schedule of 45 °C/1 h + 90 °C/1 h + 115 °C/0.5 MPa/1 h + 150 °C/0.5 MPa/1 h + 177 °C/0.5 MPa/3 h. The final unidirectional CFRP laminate had a thickness of 15 mm. The sample thickness for the steady-state heat flow method was controlled at 7 mm.

### 2.3 Measurement of Thermal Conductivity

According to ASTM E1461, the sample dimensions for LFA measurement are recommended to be 12.7 mm as a diameter and 6 mm or less as a thickness. The LFA sample was prepared by stacking a group of bars machined from composite material, and further machined into round

**Table 1** Properties of carbon fiber and AG80

Material	Density/g/cm <sup>3</sup>	Specific Heat/J/(g·K)	Thermal conductivity/W/(m·K)	
			Axial	Radial
XN-90-60S	2.19	0.7	500	10
High-modulus carbon fiber	1.85	0.7	66	10
AG80	1.26	1.0	0.19	

samples, thus ensuring the in-plane direction of interest along the samples' thickness direction. The samples were shaped to a diameter of 12.7 mm.

The thermal diffusivity was measured by an LFA 447 machine (Netzsch) stably at 300 K in an argon atmosphere. In the measurement, a flash pulse with length  $t_{pulse}$  was generated by a Xenon gas flash tube. The  $t_{pulse}$  should be set less than one-fifth of  $t_{1/2}$ , which is the period of temperature reaching half the maximum. The flash pulse was evenly emitted to the bottom surface of the composite sample to yield a heat pulse. Temperature changes at the central area of the top surface were recorded with an infrared detector. For one-dimensional through-thickness heat transfer, the thermal diffusivity and thermal conductivity can be calculated by Eqs. (1 and 2) [22].

$$\alpha = \frac{0.139L^2}{t_{1/2}} \quad (1)$$

$$\lambda = \alpha \cdot c_p \cdot \rho \quad (2)$$

Here, we define the measured thermal conductivity at a specific geometry as the apparent thermal conductivity. The sample specific heat was measured in a nitrogen atmosphere by a differential scanning calorimetry (Mettler Toledo). The density was measured by an ME104 Balance (Mettler Toledo) based on Archimedes' law. The specific heat and density were measured to be  $0.75 \pm 0.04$  J/(g·K) and  $1.80 \pm 0.04$  g/cm<sup>3</sup> for the tested sample.

In addition, a steady-state heat flow method was conducted according to ASTM D5470-12 by using an LW-9389 (Taiwan Long Win Science and Technology Corporation). The samples were sandwiched by two copper blocks at temperatures of 300 K and 350 K. The interfacial thermal resistances between the samples and copper blocks were eliminated by measuring two samples with different thicknesses. The apparent thermal conductivity in the heat flow direction can be calculated by Fourier's Law, as follows:

$$q = -\lambda \frac{\Delta T}{l} \quad (3)$$

Where  $q$  is the areal density of the heat flow rate,  $\lambda$  is the thermal conductivity,  $\Delta T$  is the temperature gradient ( $\Delta T = T_1 - T_2$ ), and  $l$  is the sample length in the heat flow direction.

### 3 Simulation of Heat Transfer

A heat transfer simulation was conducted using the Abaqus finite element package. The simulation of heat transfer was based on the following hypotheses: (1) The contact thermal resistance between the carbon fiber and epoxy matrix was negligible. (2) Thermal expansion and thermal stress were ignored. (3) The porosity of unidirectional CFRP was assumed to be zero.

For LFA measurement, representative volume element (RVE) models were constructed with the same radius-to-thickness ratio,  $r/z$ , as the experimental samples. Material properties were assigned to the RVE models, including the density, specific heat, and thermal conductivity of the carbon fiber and the epoxy matrix. An initial temperature of 300 K was set for the RVE models. A heat pulse with a pulse length of  $10^{-8}$  s and heat flow density of  $10^{10}$  W/m<sup>2</sup> were evenly applied on the bottom surface of the RVE models. According to the simulative

results,  $10^{-8}$  s was less than one-fifth of  $t_{1/2}$  for the current simulation. It should be pointed out that the deviation of thermal diffusivity was as low as 0.55% with and without considering radiation, and thus the heat loss by radiation was ignored in this research. The RVE models were meshed by DC3D10 to ensure no more than 0.01% of the grids had a tri-face corner angle of less than  $5^\circ$ . Meanwhile, the eccentric geometric factor of all grids was under 0.2. By applying the Abaqus package, the computation would end once the variation rate of the temperature was less than  $10^{-3}$  K/s. The simulative temperature-time curves at the central area of the top surface were then used to obtain  $t_{1/2}$ . Consequently, the thermal diffusivity and apparent thermal conductivity of the RVE models were calculated by Eqs. (1 and 2).

For the steady-state heat flow method, the RVE models were also designed to have the same aspect ratio as the experimental samples. The top and bottom surfaces of the models were set two constant-temperature fields of 350 K and 300 K. Other surfaces were set as insulated. The models were meshed into proper numbers of DC3D10 grids. The areal density of the heat flow rate was recorded to calculate the thermal conductivity in the direction of the heat flow by using Fourier’s Law.

## 4 Results and Discussion

### 4.1 Apparent Thermal Conductivity of Unidirectional CFRP along Different In-plane Orientations

Figure 1 shows the variations of the measured thermal conductivity along different in-plane orientations of unidirectional CFRP. The cylinder sample was fabricated to ensure a direction of interest along its thickness direction for LFA measurement. The sample has a diameter of 12.7 mm and thickness of 3.8 mm. By defining the in-plane orientation angle (i.e., the angle between the carbon fiber and heat conductive direction) as  $\theta$ , the thermal conductivity was measured every  $15^\circ$ , as shown in Fig. 1, where  $0^\circ$  and  $90^\circ$  represent the orientations parallel or vertical to the carbon fibers. The measured thermal conductivity decreased as the orientation angle increased. In the range of  $45^\circ$  to  $60^\circ$ , a dramatic drop in the measured thermal conductivity was observed with the specific sample geometry. When the orientation angle was larger than  $45^\circ$ , the measured thermal conductivity deviated significantly from the estimated one according to the rule of mixture in Eq. (4), the Hashin Eq. (5) [28], and the Springer and Tsai Eq. (6) [29].

$$\lambda_0 = \lambda_{f,0} \cdot v_f + \lambda_m(1-v_f) \tag{4}$$

$$\lambda_{90} = \lambda_m + \frac{v_f}{\frac{1}{\lambda_{f,90}-\lambda_m} + \frac{1-v_f}{2\lambda_m}} \tag{5}$$

$$\lambda_\theta = \lambda_0 \cos^2\theta + \lambda_{90} \sin^2\theta \tag{6}$$

In order to reveal the heat conduction process along different orientation angles, RVE models were designed as shown in Fig. 2. The models were assigned a diameter of 120  $\mu\text{m}$

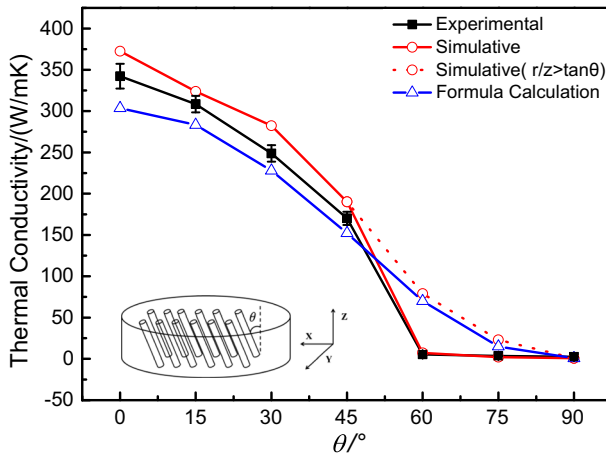


**Fig. 1** Experimental, simulative, and equation estimated results of thermal conductivity for unidirectional CFRP at different orientation angles

and a thickness of 36  $\mu\text{m}$ . The RVE models had the same radius-to-thickness ratio ( $r/z$ ) as the experimental samples. Based on cross-sectional morphology, carbon fibers were observed to be packed in a hexagonal structure, and the composite samples had a fiber volume fraction of 60.7%. The same hexagonal packing structure and fiber volume fraction were assigned to the RVE models.

Figure 3 shows the simulative temperature and time curves at the central area of the top surface. Based on these simulative temperature and time profiles, the thermal diffusivities were further obtained by Eq. (1), and thus the thermal conductivity may be further calculated as shown in Fig. 1. Although these RVE models have different orientation angles, the heat-balanced temperature on the top surface stabilized at around 323.2 K. With an increase in  $\theta$ ,  $t_{1/2}$  becomes larger, and thus the thermal diffusivity decreases. The simulative thermal conductivities coincide well with the experimental results through the entire fiber orientation from 0° to

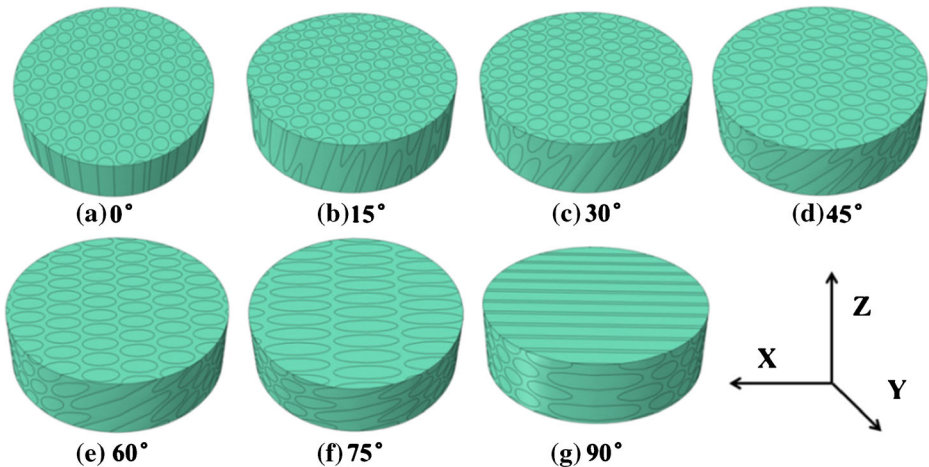


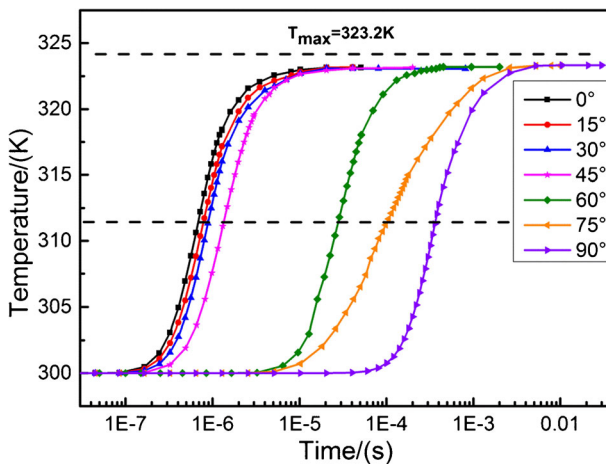
**Fig. 2** RVE models for LFA samples along different orientation angles

90°. It can be seen that both the experimental and simulative results decline dramatically in the narrow  $\theta$  range from 45° to 60°.

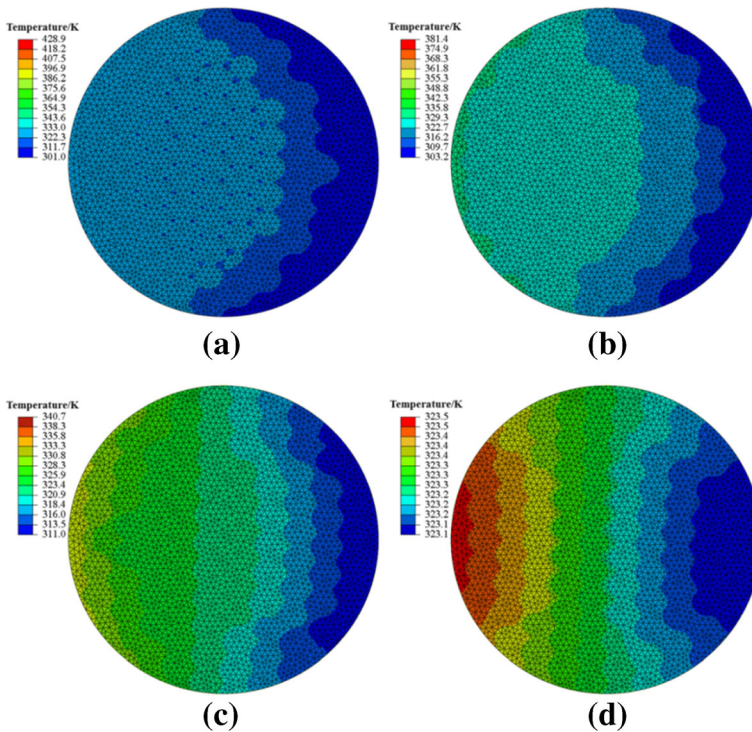
Figures 4 and 5 show the variations in the simulative temperature distribution with time on the top surfaces of RVE models with  $\theta$  of 45° and 60°, respectively. From Fig. 4, it can be observed that the heat transfer in the model with a 45° angle exhibits a two-step process. First, heat transfers through the carbon fiber along the axial direction to part of the top surface. Because of the special geometric characteristics of the RVE model, the major area of the top surface (including the central area) is heated first. At  $2.05 \times 10^{-5}$  s, the temperature of the central area is 323.0 K, which is similar to the major area of the top surface. Subsequently, heat spreads to the entire RVE model until the temperature is balanced. Since the monitoring region of the temperature in LFA measurement is the central area of the top surface, the heat transfer speed in the first step determines the apparent thermal conductivity of CFRP.

Figure 5 shows the heat transfer process for an RVE model with  $\theta$  of 60°. Although heat first transfers to the top surface through the carbon fiber along the axial direction, a limited region of the top surface shows a temperature increase owing to a less continuous conduction path of the carbon fibers through the thickness. Unlike the heat transfer process for the RVE model with  $\theta$  of 45°, the central area does not show temperature changes instantaneously. The temperature at the central area increases gradually with heat transferring from the first-heated edge region. At  $3.28 \times 10^{-4}$  s, the central area reaches a temperature of 323.0 K, which is similar to that of the major area of the top surface. The heat conduction is in a zigzag path. Therefore, in Fig. 3,  $t_{1/2}$  shows a dramatic increase from  $\theta = 45^\circ$  to  $\theta = 60^\circ$ , which accounts for the dramatic decline in the apparent thermal conductivity for both the experimental and simulative results with  $\theta$  ranging from 45° to 60°, as shown in Fig. 1. This also suggests that the apparent thermal conductivity is greatly influenced by the sample geometry, which should be received more attention when designing the ply scheme of CFRP.

Figure 6 shows the heat conduction along the individual carbon fiber filaments. The bright loop around the carbon fiber indicates the heat conduction from the fiber to the polymeric matrix. In Eq. (4), heat conduction between the fibers and matrix was neglected. This explains why the experimental thermal conductivities were larger than the estimated results for the



**Fig. 3** Variations in simulative temperature with time at central area of top surface for RVE models with  $\theta$  from 0° to 90° in LFA measurement



**Fig. 4** (a–d) Simulative temperature distribution on top surface of RVE model with  $\theta = 45^\circ$  at  $2.05 \times 10^{-5}$  s,  $4.1 \times 10^{-5}$  s,  $1.64 \times 10^{-4}$  s, and  $3.28 \times 10^{-4}$  s, respectively

equation in Fig. 1. In our simulated process, the interfacial thermal resistance, which existed in the measurement, was ignored. Therefore, the simulative thermal conductivities were larger than the experimental values, as shown in Fig. 1.

#### 4.2 Geometrical Effect on Apparent Thermal Conductivity by LFA Measurement

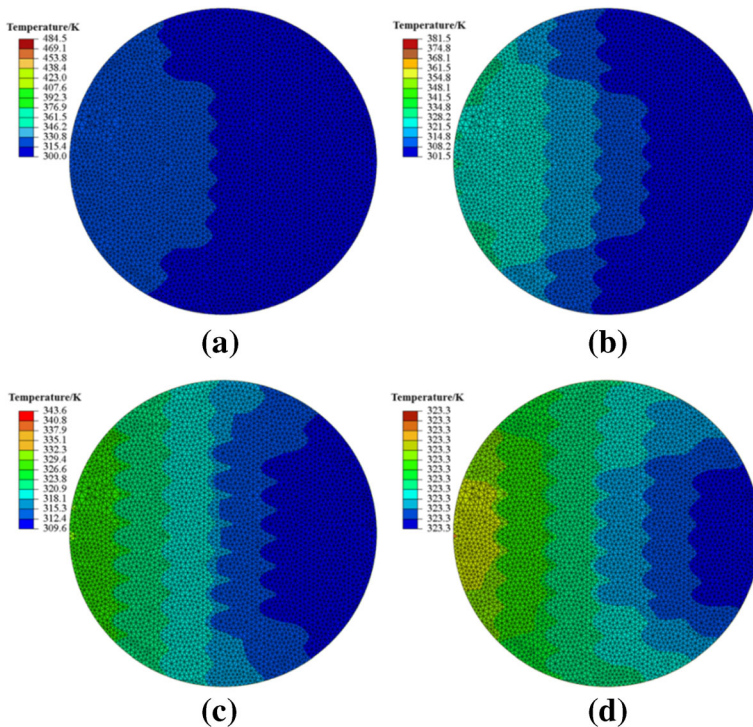
Based on the above analysis, the geometrical effect mainly occurs when  $\theta$  is between  $0^\circ$  and  $90^\circ$ . Along the axial direction of the carbon fiber (i.e.,  $\theta = 0^\circ$ ), the thermal conductivity of CFRP is dominated by the thermal conductivity of the carbon fibers. When  $\theta$  is equal to  $90^\circ$ , the heat transfer performance of CFRP is determined by a combination of the thermal conductivity of the carbon fiber along the radial direction, the fiber volume fraction, and the thermal conductivity of the matrix. The thermal conductivity of CFRP is not influenced by the sample geometry at  $\theta = 0^\circ$  or  $\theta = 90^\circ$ .

In order to reveal the geometrical effect of heat conduction, we set the RVE models with different aspect ratios. In the LFA measurement, a dimensionless shape factor was defined to describe the sample's geometric feature, which was equal to the radius-to-thickness ratio ( $r/z$ ). We set the RVE models with a diameter of  $120 \mu\text{m}$  and different thicknesses to obtain different values of  $r/z$ . Since the deviation between the estimated and experimental thermal conductivities occurred when  $\theta$  was larger than  $45^\circ$  in Fig. 1, we chose a typical  $\theta$  of  $60^\circ$  and  $75^\circ$  to investigate the influence of the geometrical structure on the apparent thermal conductivity of unidirectional CFRP.

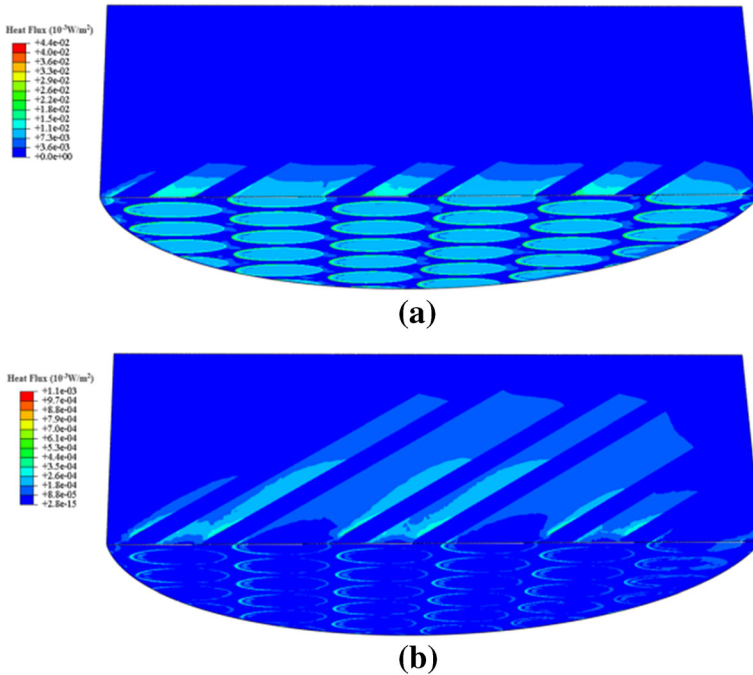


Figure 7 shows plots of FEM simulative thermal conductivities for these RVE models with different  $r/(z \cdot \tan\theta)$ . It can be seen that when  $r/z < \tan\theta$ , the simulative results of apparent thermal conductivity increase slowly. At  $r/z = \tan\theta$ , the apparent thermal conductivity shows a dramatic increase from 5.05 W/(m·K) to 76.40 W/(m·K) for  $\theta = 60^\circ$ , and that increases to 20.10 W/(m·K) for  $\theta = 75^\circ$ . When  $r/z$  becomes larger than  $\tan\theta$ , the thermal conductivities stabilize at relatively high values for both  $\theta = 60^\circ$  and  $\theta = 75^\circ$ . The corresponding theory estimation values are 72.52 W/(m·K) and 18.85 W/(m·K) at  $\theta = 60^\circ$  and  $\theta = 75^\circ$ , respectively. This indicates that Eqs. (4–6) predict the apparent thermal conductivity of unidirectional CFRP in the case of  $r/z > \tan\theta$ .

To validate the simulation in this research, the thermal conductivity of a sample with  $\theta = 60^\circ$ ,  $r = 6.3$  mm, and  $z = 2.2$  mm ( $r/z \cdot \tan\theta = 1.67$ ) was measured to be 74.2 W/(m·K), which was consistent with the simulative result of 76.40 W/(m·K). The corresponding simulative temperature distribution on the top surfaces of the RVE models with  $r/z$  of 2.89 is shown in Fig. 8, which corresponds to the case of  $r/z > \tan\theta$ . It is observed that the major areas of the top surfaces, including the central areas, are heated first, and then heat spreads to the entire RVE model until the temperature is balanced. Although in Fig. 5 the RVE model has the same diameter, it shows a completely different heat transfer process than Fig. 8. When  $r/z < \tan\theta$  in Fig. 5, heat transfers in a zigzag path, and the thermal conduction is mainly determined by the heat spreading process on the sample surface, which is determined by the thermal conductivity of the epoxy matrix and that of the carbon



**Fig. 5** (a–d) Simulative temperature distribution on top surface of RVE model with  $\theta = 60^\circ$  at 2.05e-05 s, 8.19e-05 s, 3.28e-04 s, and 7.86e-03 s, respectively



**Fig. 6** (a, b) Simulative heat flux for RVE models with  $\theta = 60^\circ$  at  $2.05e-05$  s and  $8.19e-5$  s, respectively

fiber along the radial direction. With an increase in  $r/z$ , the distance for the heat spreading process on the sample surface is shortened. This also explains the slow growth of apparent thermal conductivity when  $r/z < \tan\theta$  in Fig. 7. Moreover, when  $r/z < \tan\theta$ , the simulative thermal conductivities are very close [both around  $5.05 \text{ W}/(\text{m}\cdot\text{K})$ ] for the RVE models with  $\theta = 60^\circ$  and  $\theta = 75^\circ$ .

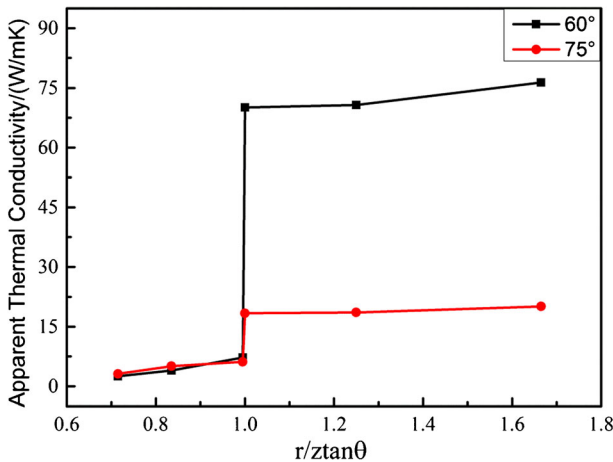


**Fig. 7** Simulative results of apparent thermal conductivity for RVE models with different  $r/z$  at  $\theta = 60^\circ$  and  $75^\circ$

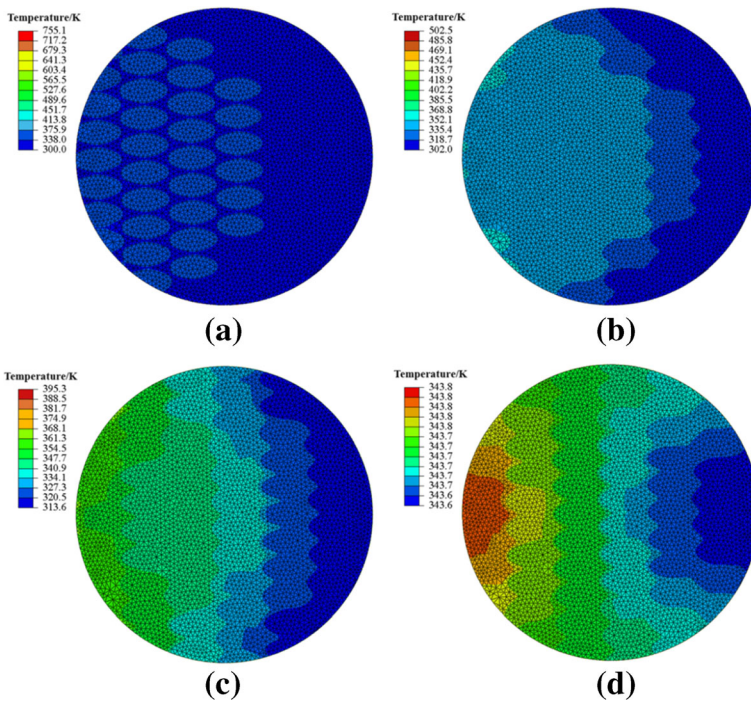


**Fig. 8** (a–d) Simulative temperature distribution on top surface of RVE model with  $\theta = 60^\circ$  and  $r/z = 2.89(r/z > \tan\theta)$  at  $5.14e-06$  s,  $2.05e-05$  s,  $8.19e-05$  s, and  $7.86e-03$  s, respectively

### 4.3 Geometrical Effect on Apparent Thermal Conductivity in Steady-State Heat Flow Measurement

The geometrical effect on the apparent thermal conductivity of anisotropic fiber-reinforced composite was also investigated based on the steady-state heat flow method. Figure 9 shows

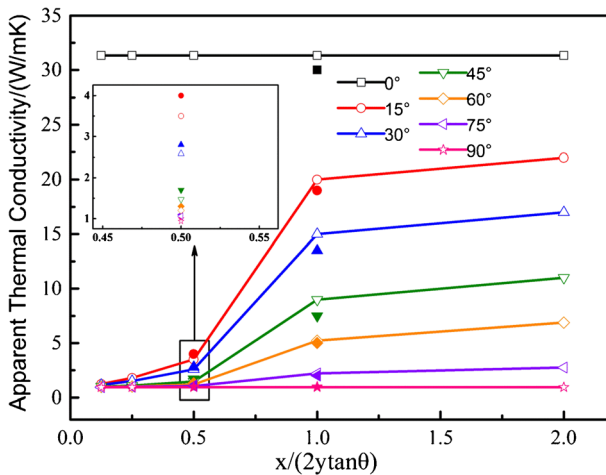


**Fig. 9** Variations in apparent thermal conductivity with  $x/(2ytan\theta)$  along different in-plane orientations (solid: experimental; hollow: simulative)

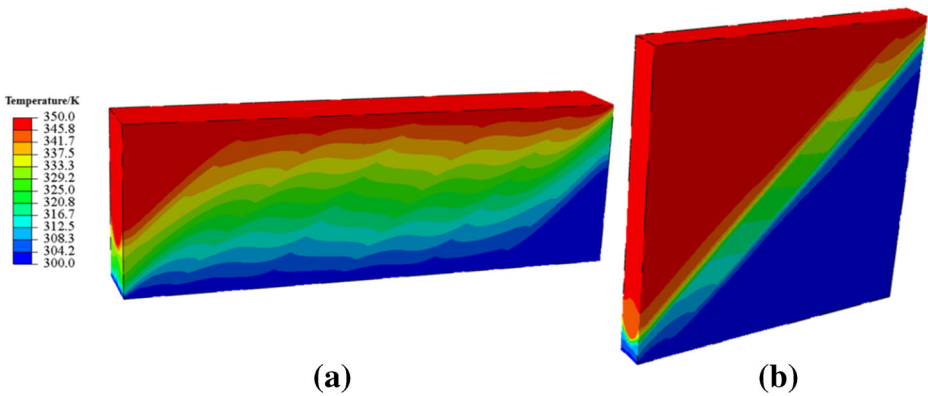


**Fig. 10** Simulative temperature distribution for CFRP with orientation angle of  $45^\circ$  by steady-state heat flow method: (a)  $x/(2y\tan\theta) = 2$ , (b)  $x/(2y\tan\theta) = 0.5$

the dependency of the apparent thermal conductivity on the sample's geometry. In this case, the shape factor of a rectangular sample is equal to  $x/2y$ , where  $x$  and  $y$  represent the sample dimensions perpendicular and parallel to the heat transfer direction. The heat transfer is simulated at different in-plane orientation angles with  $x/(2y\tan\theta)$  of 0.25, 0.5, 1, and 2. It can be seen in Fig. 9 that the apparent thermal conductivity increases with increasing  $x/(2y\tan\theta)$ , except for the samples with fiber orientations of  $0^\circ$  or  $90^\circ$  (fiber parallel or perpendicular to the temperature gradient). When  $\theta$  is  $0^\circ$  or  $90^\circ$ , the apparent thermal conductivity has constant maximum and minimum values, respectively. When  $\theta$  is between  $0^\circ$  and  $90^\circ$ , a moderate increase in the apparent thermal conductivity is observed at small  $x/(2y\tan\theta)$ , which is followed by a dramatic increase at  $x/(2y\tan\theta) = 1$ . When  $x/(2y\tan\theta)$  becomes larger than 1, the apparent thermal conductivity tends to match the theoretically estimated results according to Eq. (4–6). The simulated results (hollow points) are also verified by the experimental results (solid points) in Fig. 9. This phenomenon is similar to that of the LFA measurement. This suggests the geometrical effect is a common feature for anisotropic CFRP in both transient and steady-state heat flow processes. A reasonable ply scheme is the key to fully exploiting the fiber's thermal conductivity performance in the final composites.

In order to further reveal the heat transfer in the steady-state heat flow method, temperature distributions with a typical fiber orientation angle of  $45^\circ$  are shown in Fig. 10. In Fig. 10(a) and (b),  $x/(2y\tan\theta)$  was set to be 2 and 0.5, respectively. When  $x/(2y\tan\theta) = 2$ , it can be seen that the carbon fiber established a continuous heat transfer path between the two surfaces along the temperature gradient. If  $x/(2y\tan\theta)$  become slower than 1, heat is unable to transfer directly between the two surfaces through the carbon fiber's axial direction. Heat was conducted via a polymeric matrix and the fiber's radial direction. The tortuous heat conduction path and low thermal conductivity of the matrix caused a lower apparent thermal conductivity.

## 5 Conclusions

The thermal conductivity of unidirectional CFRP in different in-plane orientations was investigated by laser flash analysis and a steady-state heat flow method, and the heat transfer process was simulated to explore the geometrical effect on thermal conduction. It was found that the geometry of unidirectional CFRP significantly affects the apparent thermal

conductivity when  $\theta$  is between  $0^\circ$  and  $90^\circ$ . In the LFA measurement when the radius-to-thickness ratio was larger than  $\tan\theta$ , the simulative thermal conductivities agreed well with the theoretical estimation values. When the radius-to-thickness ratio was close to  $\tan\theta$ , the apparent thermal conductivity showed a dramatic decline. For the sample with a radius-to-thickness ratio of less than  $\tan\theta$ , the simulative thermal conductivities showed slow growth with an increase in the radius-to-thickness ratio around a low value, which seriously deviated from the theoretical estimation values. Based on finite element analysis, this phenomenon was revealed to correlate with a change in the heat transfer process from a continuous path to a zigzag path. An optimal ply scheme may fully exploit the fiber's thermal conductivity performance in composite laminate. In addition, radial heat transfer between the fiber and matrix was found to cause a lower theory estimation value than the experimental thermal conductivity, while ignoring the interface thermal resistance led to a higher simulative value than the experimental thermal conductivity.

**Acknowledgements** The authors acknowledge the financial support from the National Natural Science Foundation of China (51403009).

## References

1. Soutis, C.: Carbon fiber reinforced plastics in aircraft construction. *Mater. Sci. Eng. A*. **412**(1-2), 171–176 (2005). <https://doi.org/10.1016/j.msea.2005.08.064>
2. Ye, L., Lu, Y., Su, Z., Meng, G.: Functionalized composite structures for new generation airframes: a review. *Compos. Sci. Technol.* **65**(9), 1436–1446 (2005). <https://doi.org/10.1016/j.compscitech.2004.12.015>
3. Egan, B., McCarthy, C.T., McCarthy, M.A., Gray, P.J., O'Higgins, R.M.: Static and high-rate loading of single and multi-bolt carbon–epoxy aircraft fuselage joints. *Compos. A: Appl. Sci. Manuf.* **53**, 97–108 (2013). <https://doi.org/10.1016/j.compositesa.2013.05.006>
4. Silva, C.A., Marotta, E., Schuller, M., Peel, L., O'Neill, M.: In-Plane Thermal Conductivity in Thin Carbon Fiber Composites. *J. Thermophys. Heat Transf.* **21**(3), 460–467 (2007). <https://doi.org/10.2514/1.27859>
5. Frusteri, F., Leonardi, V., Vasta, S., Restuccia, G.: Thermal conductivity measurement of a PCM based storage system containing carbon fibers. *Appl. Therm. Eng.* **25**(11-12), 1623–1633 (2005). <https://doi.org/10.1016/j.applthermaleng.2004.10.007>
6. Yu, H., Nonn, A., Schneiders, S., Heider, D., Advani, S.G.: An approach to enhance through-thickness thermal conductivity of polymeric fiber composites. *Int. J. Heat Mass Transf.* **59**, 20–28 (2013). <https://doi.org/10.1016/j.ijheatmasstransfer.2012.11.055>
7. Sweeting, R.D., Liu, X.L.: Measurement of thermal conductivity for fibre-reinforced composites. *Compos. A: Appl. Sci. Manuf.* **35**(7-8), 933–938 (2004). <https://doi.org/10.1016/j.compositesa.2004.01.008>
8. Yin, J.J., Chang, F., Li, S.L., Yao, X.L., Sun, J.R., Xiao, Y.: Lightning Strike Ablation Damage Influence Factors Analysis of Carbon Fiber/Epoxy Composite Based on Coupled Electrical-Thermal Simulation. *Appl. Compos. Mater.* **24**(5), 1089–1106 (2016). <https://doi.org/10.1007/s10443-016-9577-1>
9. Kandare, E., Khatibi, A.A., Yoo, S., Wang, R., Ma, J., Olivier, P., Gleizes, N., Wang, C.H.: Improving the through-thickness thermal and electrical conductivity of carbon fibre/epoxy laminates by exploiting synergy between graphene and silver nano-inclusions. *Compos. A: Appl. Sci. Manuf.* **69**, 72–82 (2015). <https://doi.org/10.1016/j.compositesa.2014.10.024>
10. Han, S., Chung, D.D.L.: Increasing the through-thickness thermal conductivity of carbon fiber polymer–matrix composite by curing pressure increase and filler incorporation. *Compos. Sci. Technol.* **71**(16), 1944–1952 (2011). <https://doi.org/10.1016/j.compscitech.2011.09.011>
11. Pérez-Grande, I., Sanz-Andrés, A., Guerra, C., Alonso, G.: Analytical study of the thermal behaviour and stability of a small satellite. *Appl. Therm. Eng.* **29**(11-12), 2567–2573 (2009). <https://doi.org/10.1016/j.applthermaleng.2008.12.038>
12. Yuan, G., Li, X., Dong, Z., Westwood, A., Cui, Z., Cong, Y., Du, H., Kang, F.: Graphite blocks with preferred orientation and high thermal conductivity. *Carbon.* **50**(1), 175–182 (2012). <https://doi.org/10.1016/j.carbon.2011.08.017>

13. Lee, G.-W., Park, M., Kim, J., Lee, J.I., Yoon, H.G.: Enhanced thermal conductivity of polymer composites filled with hybrid filler. *Compos. A: Appl. Sci. Manuf.* **37**(5), 727–734 (2006). <https://doi.org/10.1016/j.compositesa.2005.07.006>
14. Marques, S.P.C., Barbero, E.J., Murillo, J.S.R.: Analysis of conduction-radiation problem in absorbing and emitting nongray materials. *Int. J. Num. Methods Heat Fluid Flow.* **19**(2), 165–181 (2009). <https://doi.org/10.1108/09615530910930955>
15. Babapoor, A., Azizi, M., Karimi, G.: Thermal management of a Li-ion battery using carbon fiber-PCM composites. *Appl. Therm. Eng.* **82**, 281–290 (2015). <https://doi.org/10.1016/j.applthermaleng.2015.02.068>
16. Wang, M., Kang, Q., Pan, N.: Thermal conductivity enhancement of carbon fiber composites. *Appl. Therm. Eng.* **29**(2–3), 418–421 (2009). <https://doi.org/10.1016/j.applthermaleng.2008.03.004>
17. Park, J.G., Cheng, Q., Lu, J., Bao, J., Li, S., Tian, Y., Liang, Z., Zhang, C., Wang, B.: Thermal conductivity of MWCNT/epoxy composites: The effects of length, alignment and functionalization. *Carbon.* **50**(6), 2083–2090 (2012). <https://doi.org/10.1016/j.carbon.2011.12.046>
18. Shigang, A., Rujie, H., Yongmao, P.: A Numerical Study on the Thermal Conductivity of 3D Woven C/C Composites at High Temperature. *Appl. Compos. Mater.* **22**(6), 823–835 (2015). <https://doi.org/10.1007/s10443-015-9438-3>
19. Zhao, Y., Song, L., Li, J., Jiao, Y.: Multi-Scale Finite Element Analyses of Thermal Conductivities of Three Dimensional Woven Composites. *Appl. Compos. Mater.* (2017). <https://doi.org/10.1007/s10443-017-9601-0>
20. Fujita, R., Nagano, H.: Novel fiber orientation evaluation method for CFRP/CFRTP based on measurement of anisotropic in-plane thermal diffusivity distribution. *Compos. Sci. Technol.* **140**, 116–122 (2017). <https://doi.org/10.1016/j.compscitech.2016.12.006>
21. McIvor, S.D., Darby, M.I., Wostenholm, G.H., Yates, B., Banfield, L., King, R., Webb, A.: Thermal conductivity measurements of some glass fibre- and carbon fibre-reinforced plastics. *J. Mater. Sci.* **25**(7), 3127–3132 (1990)
22. Parker, W.J., Jenkins, R.J., Butler, C.P., Abbott, G.L.: Flash Method of Determining Thermal Diffusivity, Heat Capacity, and Thermal Conductivity. *J. Appl. Phys.* **32**(9), 1679 (1961). <https://doi.org/10.1063/1.1728417>
23. Hind, S., Robitaille, F.: Measurement, modeling, and variability of thermal conductivity for structural polymer composites. *Poly. Comp. NA-NA.* (2009). <https://doi.org/10.1002/pc.20867>
24. McMasters, R.L., Dinwiddie, R.B.: Anisotropic Thermal Diffusivity Measurement Using the Flash Method. *J. Thermophys. Heat Transf.* **28**(3), 518–523 (2014). <https://doi.org/10.2514/1.4189>
25. Alway-Cooper, R.M., Theodore, M., Anderson, D.P., Ogale, A.A.: Transient heat flow in unidirectional fiber-polymer composites during laser flash analysis: Experimental measurements and finite element modeling. *J. Compos. Mater.* **47**(19), 2399–2411 (2012). <https://doi.org/10.1177/0021998312458130>
26. Hu, N., Chiang, S.W., Yi, J., Li, X., Li, J., Du, H., Xu, C., He, Y., Li, B., Kang, F.: Prediction of interfacial thermal resistance of carbon fiber in one dimensional fiber-reinforced composites using laser flash analysis. *Compos. Sci. Technol.* **110**, 69–75 (2015). <https://doi.org/10.1016/j.compscitech.2015.01.025>
27. Ishizaki, T., Nagano, H.: Measurement of Three-Dimensional Anisotropic Thermal Diffusivities for Carbon Fiber-Reinforced Plastics Using Lock-In Thermography. *Int. J. Thermophys.* **36**(10–11), 2577–2589 (2014). <https://doi.org/10.1007/s10765-014-1755-5>
28. Hashin, Z.: Analysis of composite materials-a survey. *J. Appl. Mech.* **50**, 3, 481–505 (1983)
29. Springer, G.S., Tsai, S.W.: Thermal conductivities of unidirectional materials. *J. Compos. Mater.* **1**, 2, 166–173 (1967)